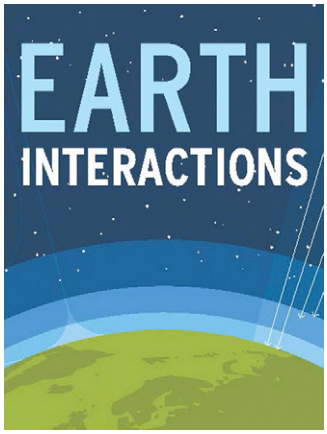

On the Nature of Temporal Variability of the Gulf Stream Path from 75° to 55°W

Avijit Gangopadhyay

School for Marine Science and Technology, University of Massachusetts Dartmouth, Fairhaven, Massachusetts

Ayan H. Chaudhuri*

Atmospheric and Environmental Research, Inc., Lexington, Massachusetts

Arnold H. Taylor

Plymouth Marine Laboratory, and School of Mathematics and Statistics, University of Plymouth, Plymouth, United Kingdom

Received 1 May 2015; in final form 19 November 2015

ABSTRACT: The response of the Gulf Stream (GS) system to atmospheric forcing is generally linked either to the basin-scale winds on the subtropical gyre or to the buoyancy forcing from the Labrador Sea. This study presents a multiscale synergistic perspective to describe the low-frequency response of the GS system. The authors identify dominant temporal variability in the North Atlantic Oscillation (NAO), in known indices of the GS path, and in the

* Corresponding author address: Ayan H. Chaudhuri, Atmospheric and Environmental Research, Inc., 131 Hartwell Ave., Lexington, MA 02421.
E-mail address: achaudhu@aer.com

DOI: 10.1175/EI-D-15-0025.1

observed GS latitudes along its path derived from sea surface height (SSH) contours over the period 1993–2013. The analysis suggests that the signature of interannual variability changes along the stream's path from 75° to 55°W. From its separation at Cape Hatteras to the west of 65°W, the variability of the GS is mainly in the near-decadal (7–10 years) band, which is missing to the east of 60°W, where a new interannual (4–5 years) band peaks. The latter peak (4–5 years) was missing to the west of 65°W. The region between 65° and 60°W seems to be a transition region. A 2–3-yr secondary peak was pervasive in all time series, including that for the NAO. This multiscale response of the GS system is supported by results from a basin-scale North Atlantic model. The near-decadal response can be attributed to similar forcing periods in the NAO signal; however, the interannual variability of 4–5 years in the eastern segment of the GS path is as yet unexplained. More numerical and observational studies are warranted to understand such causality.

KEYWORDS: Circulation/dynamics; Ocean circulation; Ocean dynamics; Atmosphere/ocean structure/phenomena; Atmosphere–ocean interaction; North Atlantic Oscillation

1. Introduction

The Gulf Stream (GS) system, a major oceanic feature in the North Atlantic, spans a large spatial extent. It starts as the Florida Current along the southeastern shores of the United States, where it is composed of the wind-driven western boundary current (WBC) and of the Loop Current in the Gulf of Mexico turning around the tip of Florida. Between 25° and 35°N, over a distance of 1000 km, it gathers transport to grow from a 25-Sverdrup (Sv; 1 Sv = 10^6 m^3 s^{-1}) current to a 90-Sv (Halkin and Rossby 1985) energetic stream. This northward WBC then separates from the coast near 35°N, 75°W and meanders northeastward. Between 75° and 65°W, over a distance of almost 1000 km, the GS has large-scale (long wavelength) meanders. It is in this region, where instabilities grow and propagate to the east, that more rings get reabsorbed than form (Lee and Cornillon 1996).

From 60° to 45°W, over the next 1500 km of its path, the GS generates large-amplitude meanders and forms frequent eddies on both sides (warm- and cold-core rings; Brown et al. 1986; Cornillon 1986; Cornillon et al. 1987). Farther west, between 75° and 60°W, the stream is joined by recirculation from the south and from the north (Hogg 1992; Gangopadhyay et al. 1997), which adds transport to reach a maximum of 150 Sv at 60°W. East of 60°W, the stream loses part of its transport via ring formation and mass exchanges by feeding the recirculation gyres on both sides. In addition, the stream loses part of its transport to the slope current flowing to the northeast around 55°W (Fratantoni and Pickart 2007).

One would thus expect that such a large-scale system, which spans almost 4000 km in the Atlantic basin, would respond in a complex manner to the large-scale atmospheric system that overlies this ocean and the underlying thermohaline circulation. The large spatial extent of the stream might not respond to the overlying wind field as a single entity. In fact, different segments of the stream may respond differently to the large-scale wind pattern, which is often represented by a single index, the North Atlantic Oscillation (NAO). Quantifying the dynamical linkages between the NAO and different parts of the GS would be a challenging undertaking, and the reader is referred to a recent historical perspective of such

challenges described by Taylor (2011). Our focus here is on the possibility of different time scales in the response signal of the GS along its path. Specifically, we propose to address a single primary question: Does the Gulf Stream system respond at different temporal scales east and west of 60°–65°W? And, if so, might these different time scales relate to the different forcing mechanisms mentioned above? We present evidence for an affirmative answer using past observations and available model results.

The thermohaline linkage between the GS and the atmosphere is rather indirect. It is affected by convection in the Labrador Sea (Myers et al. 1989; Dickson et al. 1996) and subsequent advection of Labrador Sea Water (LSW) in the upper branches of the deep western boundary current (DWBC) in the slope waters south of the tail of the Grand Banks (Pickart et al. 1999) and via the Labrador Current (LC) around the tail of the Grand Banks (Smith et al. 2001). The time scales of this interrelationship remain somewhat elusive. Many of the recent studies (Rossby 1999; Rossby and Benway 2000; Drinkwater et al. 2003; Drinkwater 2004; Hameed and Piontkovski 2004) have focused their attention on the lag time scale between the advection from the Labrador Sea and the latitudinal variation of the GS path. Mechanisms such as forcing by the DWBC (Thompson and Schmitz 1989; Spall 1996) and the movement of the Icelandic low (Hameed and Piontkovski 2004) have been suggested. However, recent observational evidence by Bower et al. (2009) showed that most of the southward flow from the Labrador region follows an interior pathway in the subtropical gyre (from south of 50°N to the western boundary at 32°N), different from that of the prevalent DWBC pathway.

The coupling between the ocean and atmosphere is more direct for wind-driven currents. Gangopadhyay et al. (1992) corroborated the Parsons–Veronis (Parsons 1969; Veronis 1973) hypothesis relating the integrated Ekman drift to the separation of the GS at Cape Hatteras using satellite observations from 1977 to 1988. This was further supported by the GS north wall (GSNW) analyses carried out by Taylor and Stephens (1998, hereafter TSI), which linked the GSNW index (over 75°–65°W) during 1966–96 with the wind forcing over the North Atlantic as represented by the NAO.

Joyce et al. (2000) defined a different GSNW index based on subsurface temperature at 200-m depth. They presented a feedback mechanism to explain the commonly observed decadal variability in the linked system of the subtropical mode water, SST, GS position, and the NAO. In a subsequent study, Frankignoul et al. (2001) analyzed the TOPEX/Poseidon altimeter data from October 1992 through November 1998 to define the lead and lag time between the GS path and sea level pressure, wind stress, and SST. They found a fast-response lag time of 1 year, attributable to the buoyancy forcing by the recirculation gyres, and a slow-response lag time of 9 years, attributable to large-scale wind stress forcing. Their study could not validate the notion of the GS impacting the large-scale atmosphere, as was hypothesized by Joyce et al. (2000). Eden and Willebrand (2001) used a ⅓° model with 45 levels and showed that intense convection-related activities in the Labrador Sea might impact the GS system with time scales of 6–8 years.

The present paper uses the NAO winter index as a guide to the characteristic time scales of the variability of the North Atlantic atmosphere. It is well known that the strength of the NAO does directly influence the North Atlantic Ocean (Walker and

Bliss 1932; Hurrell et al. 2000, 2001). The NAO index itself has a rich blend of low frequencies. Cook et al. (1998) found concentrations of spectral power around periods of 24, 8, and 2 years; however, they also identified a multidecadal signal at 70 years. It is worth noting at this time that Wunsch (1999) cautioned regarding the interpretation of short climate records such as that of the NAO; he also found extra energy and peaks at 7–10 years and 2–3 years.

One of the limiting factors in analyzing the climatic signals of the GS system is the limited/restricted length of the available datasets. The conventional Fourier transform (FT) approach is often inapplicable to short as well as gappy (spatially and temporally) datasets or, when applicable, provides dubious results. Gangopadhyay et al. (1989) suggested an alternative methodology for analyzing such oceanographic datasets by using an autoregressive (AR) spectral analysis technique (Kay and Marple 1981). The applicability of the AR methodology to finite length time series is presented in the next section. The observed variability in the GS system signatures is then described in section 3 and compared with an analysis of the NAO time series. Section 4 presents additional results from the ⅛° basin-scale ocean model of Chaudhuri et al. (2011a,b), which allows us to understand the behavior of the GS for representative low and high NAO periods. Finally, section 5 discusses a number of possible reasons for the differences between the eastern and western parts of the GS and presents a synergistic perspective to account for these differences.

2. Application of AR analyses to finite length datasets

Gangopadhyay et al. (1989) compared the AR method with FT analysis for five case studies. The length of those datasets ranged from 17 to 98 points. These included (i) a 98-point GS path spatial series for wavenumber detection, (ii) a modified GS path with a 25-point gap introduced within (i), (iii) a 64-point simulated time series with two closely spaced wavenumbers, (iv) a 55-point subtropical convergence zone (STCZ) SST time series, and (v) a 17-point wind energy time series. Their study found that as the length of time series decreases, the resolving power of AR method increases considerably compared to that of FT method. Specifically, while for the longest dataset (98 points) the AR method performed slightly better (in identifying a sharper peak and providing a smoother spectra) than the FT, for the short ones (17 and 55 points) the AR method showed a dramatic improvement over conventional FT.

As discussed by Gangopadhyay et al. (1989), three important issues when applying the AR technique are selection of the model order, sensitivity of the spectral peak locations to the selected order, and determination of the confidence interval for the resolved spectral peaks. We summarize the general results from that study here and address these particular issues for the GS indices and path series as applicable later in section 3.

There are several algorithms available to solve the model coefficients of an AR model (Press et al. 1986). Although different statistical criteria, including final prediction error (FPE), criterion autoregressive transfer (CAT) function (Koslov and Jones 1985), and the minimum description length (MDL) (Rissanen 1983), are available, Gangopadhyay et al. (1989) followed the subjective method of looking at the ‘‘fall of reflection coefficients’’ in their analysis for selecting the order. They

maintained that this helped to identify real peaks in the signal. This subjectivity was supported by two factors: 1) there is no consistent statistical criterion for short datasets (S. M. Kay 1987, unpublished data), and 2) the reflection coefficient sequence is related to the model coefficient vector by so-called step-up and step-down algorithms (Jackson 1986). However, as a rule of thumb, it is best not to choose an order greater than $N/3$ and to restrict the orders to four or eight with oceanographic datasets that are less than 100 points long. As explained later (section 3), based on the nature of fall of reflection coefficients and to be consistent in dealing with short but different datasets, we have used an order of eight to obtain the spectra from all of the presented time series.

Note that all of the time series spectrally analyzed in this study were standardized in the following way so that their spectral estimates could be compared. First, each of the time series was detrended to remove very low-frequency signal (if any). Then, each time series was divided by its standard deviation after the mean was removed. These operations had the effect of transforming the data into a set of observations with unit standard deviation (and zero mean, detrended) before applying the spectral analysis.

The confidence interval (CI) for spectral estimates by AR methodology is based on approximate statistics and remains constant across the spectrum because of the form of variance (Kay and Marple 1981). It depends on the factor $(2p/N)^{1/2}$ for a pth-order model of an N-point series. While there are rigorous methods for estimating the CI (Koslov and Jones 1985), the energy level of the individual peaks can be used subjectively for qualitative significance of the spectral signature. We followed the methodology described by Equation (6.4.20) of Jenkins and Watts (1968, hereafter JW68), and the results are described in section 3.

In this study, several spectral plots are analyzed. We have used the Burg (1977) algorithm provided in the MATLAB scientific toolbox. Using the Bartlett window formulation (Table 6.6 of JW68), the number of degrees of freedom ν for an N-point time series and a pth-order AR model is determined to be $3N/p$. The requirement of high CI demands large degrees of freedom or large sample size. Moreover, the shorter the time series (less degrees of freedom), the wider is the bound of the CI due to the character of the t-distribution (see Figure 3.10 of JW68). For the finite length (21–41 points) datasets presented herein, most of the spectral peaks are found to be significant at 90% CI except two, which are the 5-yr peak for the NAO (1966–2006) series, and the 5-yr peak for the AVISO GS series for 60°W. For this reason, we have presented both 80% and 90% CI bounds for all spectral plots presented in Figures 1, 3, and 4 below.

3. Low-frequency variability of the observed Gulf Stream system

To understand the low-frequency variation of the GS path, we analyzed three different datasets available from different sources. These are 1) the GS North Wall (GSNW) index from TSI; 2) the GSNW quarterly index computed by Joyce et al. (2009, hereafter JQI); and 3) the annual mean path of the GS based on 50-cm sea surface height (SSH) contours as derived from the last 21 years (1993–2013) of AVISO altimetry data. Note that both the TSI and JQI are composite indices, in that

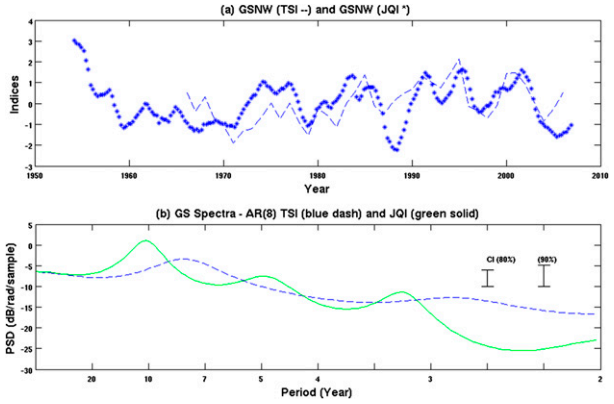

Figure 1. (a) Time series of Joyce index (marked with asterisks) and Taylor–Stephens GSNW index (dashed line). (b) Eighth-order AR spectrum of the TSI (blue dashed) and JQI (green solid). All of the peaks are significant at 90% CI, except the 3-yr peak for TSI.

each of them provides a single metric to represent the GS path (annual/quarterly) over a large spatial extent. The TSI was calculated by applying principal components analysis to the time series of monthly latitudes of the north wall at 79°, 75°, 72°, 70°, 67°, and 65°W (TSI). Figure 1a shows the time series (dashed line) of the TSI from 1966 to 2006. Joyce et al. (2000) constructed an alternative measure of the latitude of the GS extending back into the decade before the TSI, which they applied to the formation of mode water. This measure was derived by applying empirical orthogonal function analysis to 200 m $(15°C)^{-1}$ positions from 1955 to 1989 at nine locations [75°, 73°, 70°, 67°, 65°, 63°, 60°, 58°, and 55°W; see Figure 5 of Joyce et al. (2000)] along the GS path between 75° and 55°W. Recently, JQI have recomputed the EOFs from 1954 through 2006 on a quarterly basis, and this new index (JQI) time series is shown in Figure 1a (solid line).

Note that since the monthly index values are noisy, annual index fields were chosen for analyzing and identifying the interannual time scales of latitudinal excursion/variability. As mentioned above, TSI is computed for the surface and JQI is for the 15°C $(200\text{-m})^{-1}$ isotherm location. Given that the GS axis has a vertical tilt of about 30 km in 800 m (Tracey and Watts 1986) and the GS northern width is about 50 km (Gangopadhyay et al. 1997; and references therein), it is reasonable to assume that the annual latitudinal excursion, which is on the order of 100–300 km (depending on longitude; see Figure 2), is much greater than index error estimates.

For our analysis, we used the eighth-order AR spectrum for spectral analysis of these two indices for the common period of 1966 through 2006 (41 years). Figure 1b shows both of these spectra. Clearly, the eighth-order AR spectrum of the TSI (dashed line) is dominated by variability in the near-decadal (7–10 years) period. The eighth-order AR spectrum of the JQI (75°–55°W) shows (solid line) a near-decadal peak, with additional energy peaking in the interannual (5 and 3 years) range. It is evident from Figure 1b that the spectra from the two GS path indices differ in their peak time periods (8 and 3 years for TSI; 8, 5, and 3 years for the JQI). As an aside, while an FT analysis of both the time series (1966–2014 or their

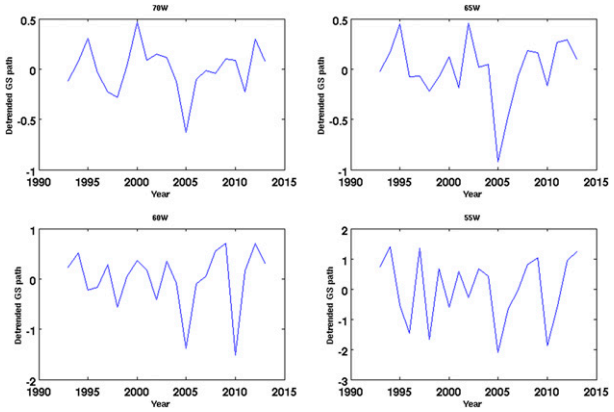

Figure 2. Time series plot for the GS path from AVISO SSHA at 70°, 65°, 60°, and 55°W. Note the apparent difference of temporal behavior west of 60°W (70° and 65°W) to those east of 60°W (60° and 55°W).

subsets 1966–2006 and 1993–2013) yielded similar peaks (not shown), the smoother AR spectra resolved sharp peaks.

Since the composite index TSI was calculated from GSNW signature between 75° and 65°W, while the composite index JQI was computed from GS path locations between 75° and 55°W, we hypothesize that the apparent discrepancies in the spectra could be explained if the GS behaved differently east and west of 60°W in response to large-scale NAO-like forcing and other factors such as its internal variability and/or interactions with Labrador inflow, topography, etc.

To investigate this hypothesis, we present a similar spectral analysis of the GS path excursions at a number of longitudes as derived from AVISO SSH anomaly fields over the last 21 years (1993–2013). Figure 2 presents the latitudinal excursions at 70°, 65°, 60°, and 55°W of the 50-cm sea surface height anomaly (SSHA) annual time series. Note the similarities of underlying temporal variability in path time series at 70°W (60°W) to that of 65°W (55°W) and the difference between the paths west (Figure 2, top panels) and east of 60°W (Figure 2, bottom panels). Figure 3 shows the eighth-order AR spectral estimate for these four longitudes. It is evident from this figure that (i) the 2–3-yr peak is apparent at all longitudes; (ii) the near-decadal peak at 8 years is seen only for 70° and 65°W and is missing east of 60°W; and (iii) the 5-yr peak is seen for 65° and eastward, while missing for 70° (Figure 3a) and 74°W (not shown). The spectrum from AVISO data at 50°W (not shown) is also very similar to those at 60° and 55°W. Note also that the AVISO dataset covers the range of longitudes used by TSI and JQI together and as such provides an independent confirmation of the longitude-based temporal variability of the GS.

A note on the sensitivity of order selection for the above spectral analysis is warranted here. Gangopadhyay et al. (1989) presented the sensitivity of the AR analysis to the selection of AR order for the short datasets of STCZ (55 points) and wind energy (17 points). The sensitivity to order selection was realized in hiding peaks for lower than optimal order and inducing spurious peaks for higher than optimal order. As suggested in that study, we used the fall of reflection coefficients' technique for the optimal order selection. From a 12-order initial AR model, we

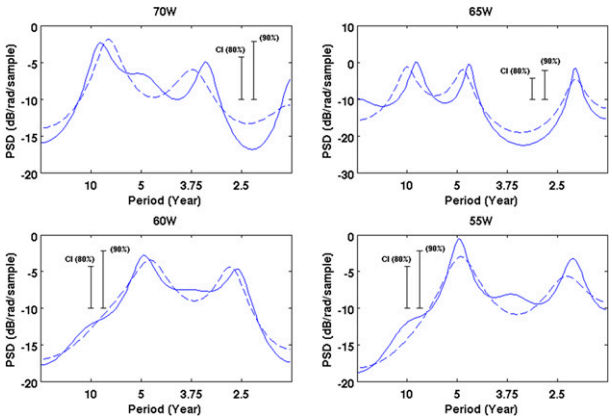

Figure 3. Spectral signatures at 70°, 65°, 60°, and 55°W from GS path time series presented in Figure 2 for 21 years (1993–2013). The solid (dash) line is for AR order 8 (6). Note the high significance of near-decadal (5 years) peaks for 70° and 65°W (60° and 55°W).

found that for the TSI and JQI, the eighth order was the right choice. However, most of the reflection coefficients for the AVISO-analyzed GS paths at 70°, 65°, 60°, and 55°W contribute up to order six or eight (not shown). Note that Gangopadhyay et al. (1989) used the sixth AR for analyzing their shortest (17 point) time series. Thus, to be consistent with the order of the GS indices analysis, we presented the eighth order AR spectra for all cases. In addition, Figure 3 presents the sixth-order (dash line) spectra for the shortest dataset (AVISO) to show the sensitivity of order selection. As expected, the sixth-order spectra shift the peaks only slightly, while the fourth-order spectra hide the higher-frequency peak (not shown). Note that all of the spectra (fourth, sixth, or eighth order) captured the 7–10-yr peak for 70° and 65°W and resolved the 5-yr peak for the 60° and 55°W GS path time series. As seen in Figures 1 and 3, all of the GS peaks (at near-decadal and 5-yr periods) are significant at the 90% CI or more, except the 5-yr peak for the AVISO data at 65°W, which is significant at least at the 80% CI.

As mentioned in the introduction, we now investigate how such changes of behavior in the response of the GS might be related to the atmospheric forcing, represented by the NAO index. While this is not the only factor that influences the GS position, it is the dominant pattern of atmospheric change over the North Atlantic and so may provide a guide to the appropriate time scales. The winter NAO index time series over the analysis period (1966–2013) is shown in Figure 4a. These winter indices [December–March (DJFM)] for the NAO were obtained from Osborn (2014), which was based on the study by Jones et al. (1997). Note that spectral peaks obtained from the data on the UCAR site (Hurrell et al. 2014) are very similar. Figure 4b shows the NAO spectrum for the limited time series (1966–2006) with three distinct peaks at near-decadal (7–10 years) and interannual (5 and 3 years) time periods. These peaks match the results obtained by Wunsch (1999). Similar peaks are also obtained for the spectra of the NAO time series from 1993 to 2013, the time period for the AVISO analysis (see Figure 4c). The above results for peak significance and the very nature of

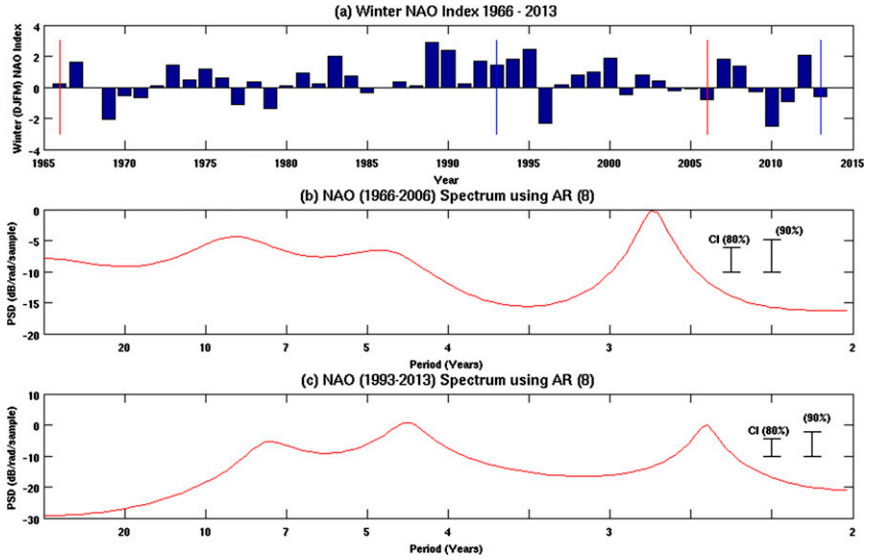

Figure 4. (a) Winter NAO index data (provided by http://www.cru.uea.ac.uk/~timo/datapages/naoi.htm). (b) Spectrum of observed NAO (1966–2006) time series with eighth-order AR. (c) Spectrum of observed NAO (1993–2013) time series with eighth-order AR. Note the presence of three peaks at 7–10-, 4–5-, and 2–3-yr bands.

the difference in the time series presented in Figure 3 demonstrate that the evidence for the spectral peaks at near-decadal and 5 years is very strong along the GS and in the NAO series.

To summarize the different spectral components in the above force-response analysis, we first note that the NAO index shows a clear near-decadal (7–10 years) peak and two other (5 and 3 years) interannual peaks. Second, it is clear from the AVISO-derived individual longitude position spectra that the near-decadal (8 years) peak is found west of 65°W but is missing to the east of 65°W; while the presence of a 5-yr peak to the east of 60°W is curious, the 3-yr peak is seen all along the GS path. Finally, while the JQI (75°–55°W index) spectra peaked at all NAO periods (8, 5, and 3 years), the TSI (75°–65°W) spectra only peaked at 8- and 3-yr periods. These different peak distributions are summarized in Table 1.

The above results suggest that the response time scales of the GS system are changing along stream, starting from about 65°W. In the next section, we examine an independent dataset, the output of a basin-scale high-resolution North Atlantic circulation model (Chaudhuri et al. 2011a,b).

4. A basin-scale model simulation for the North Atlantic

The observed difference of the GS response along its path (analyzed above) is also supported by recent results from our basin-scale modeling effort in the North Atlantic (Chaudhuri et al. 2011a,b). Two parallel 15-yr-long simulations (forced with either high or low NAO conditions of wind and heat) were carried out to understand the response of the GS to climatological (or persistent) high and low NAO

Table 1. Summary of spectral analysis from time series of GS indices, AVISO-derived paths, and NAO. Note that the significance of the 2–3-yr GS peaks is generally low.

Time series		Periods of spectral peaks		
		7–10 yr	4–5 yr	2–3 yr
GS composite index (annual/ quarterly)	TSI (75°–65°W)	✓	—	✓
	JQI (75°–55°W)	✓	✓	✓
AVISO-derived annual GS path (1993–2013)	GS path (−70°W)	✓	—	✓
	GS path (−65°W)	✓	✓	✓
	GS path (−60°W)	—	✓	✓
	GS path (−55°W)	—	✓	✓
NAO winter (DJFM) index	NAO (1966–2006)	✓	✓	✓
	NAO (1993–2013)	✓	✓	✓

conditions. The physical modeling component is based on Regional Ocean Modeling System (ROMS), which was developed and modified by Rutgers University (Song and Haidvogel 1994), University of California, Los Angeles (UCLA), and NASA/JPL scientists. Recent modifications include subgrid-scale parameterizations (Gent and McWilliams 1990; Danabasoglu et al. 1994; Griffies et al. 1998) and sigma-coordinate pressure gradient error reduction (Shchepetkin and McWilliams 2005). The North Atlantic region is simulated at ⅙° horizontal resolution and 50 vertical levels. The initial fields for the model, including temperature and salinity, are configured for the North Atlantic grid using Levitus climatology.

Detailed description of this model, its skill assessment, and relevant results were presented in Chaudhuri et al. (2011a,b). A major goal of this effort was to study the mean response of the GS to representative low and high NAO condition/forcing. This model was able to realistically reproduce the GS path (Chaudhuri et al. 2011a) and was then used to study the impact of Labrador slope/shelf water during high/low NAO periods on the path (Chaudhuri et al. 2011b).

One success criterion for the 15-yr-long high and low NAO simulations was to reproduce the high NAO versus low NAO behavior of the GSNW path, where the GSNW has been observed to be north of its mean position during high NAO years and, conversely, south of its mean position during low NAO years. Three-dimensional temperature fields from high and low NAO simulations are used to determine the mean position of the GS from 75° to 45°W. The GS mean position is estimated by initially obtaining the positions of the GS at depths of 50, 100, 200, and 400 m by following the 17°, 16°, 15°, and 12° isotherms, respectively, at 3-day intervals. The respective isotherms are subsequently integrated over depth and averaged annually for low and high NAO simulations to obtain the respective mean GS positions (see Figure 5). The simulated mean GS position is observed to be northward (southward) during persistent high (low) NAO phases, in agreement with previous work by TSI and by Taylor and Gangopadhyay (2001). It is clear from Figure 5 that this tendency of the simulated GS path is significantly realized only up to the 65°–60°W region, indicating that the decadal response of the GS west of 65°W can be attributed to the integrated effects of the NAO-like wind forcing. However, to the east of 60°W, where the simulated paths overlap considerably, the amplitude of the variability (shaded regions around the blue/red line in Figure 5) is much higher in both high and low NAO simulations than those to the

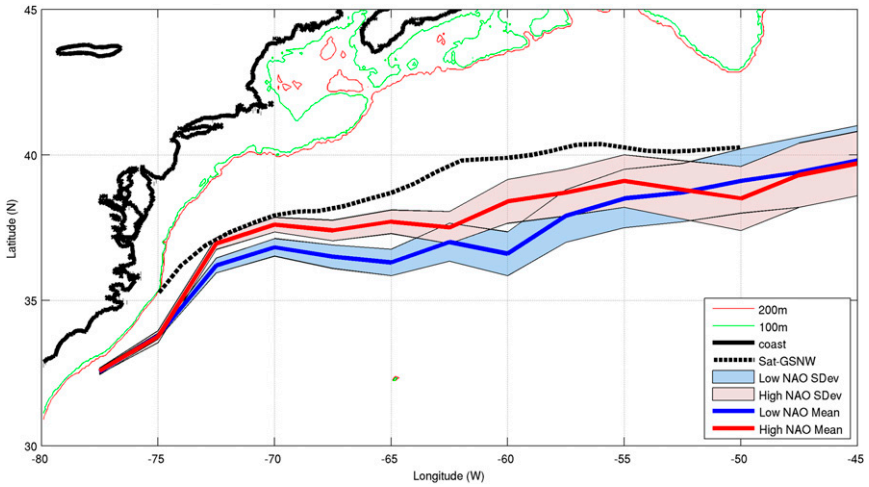

Figure 5. Annual upper layer–integrated (50–450 m) Gulf Stream positions for high (red) and low (blue) NAO simulations from the basin-scale ROMS setup. Note that (i) the mean simulated GS path between 75° and 65°W is northward (southward) during high (low) NAO periods, (ii) the simulated variability (the shaded red/blue regions around the mean path) is distinctly different west and east of 60°W for both simulations, and (iii) the region of 65°–60°W is a mixed-response, transition region.

west of 65°W. To the east of 65°W, the stream responds with more high-amplitude meandering, due to several additional processes, such as the impact of the New England seamounts, the advection from the Labrador Sea, ice melt, and the impact of the Icelandic low. The region between 65° and 60°W behaves like a transition region in the simulations, changing regimes from a wind-driven, low variability response region on the west to a mixed-response, high variability response of the GS path.

5. Discussion

The foregoing analyses suggest that during the last four decades, the GS system has behaved differently along its path from 75° to 55°W. Specifically, to the west of 60°W, the dominant variability includes time scales of 8 and 3 years, while to the east of 60°W, the dominant variability includes 5- and 3-yr time scales. However, based on the confidence intervals presented for the spectra in Figures 1 and 3, the 2–3-yr time scale should be interpreted with reservations from this annual time series analysis. We thus focus on the more significant peaks: 8 years to the west of 65°W and 5 years to the east of 60°W.

In this section, we reflect on the probable causes of these differences, which must be related to the evolution of the dynamics of meandering along the path of the stream. We propose a synergistic view, which follows the work of Stommel (1987) and is supported by our foregoing analysis (Figure 6). We designate three different regimes of variability of meandering along the GS after separation.

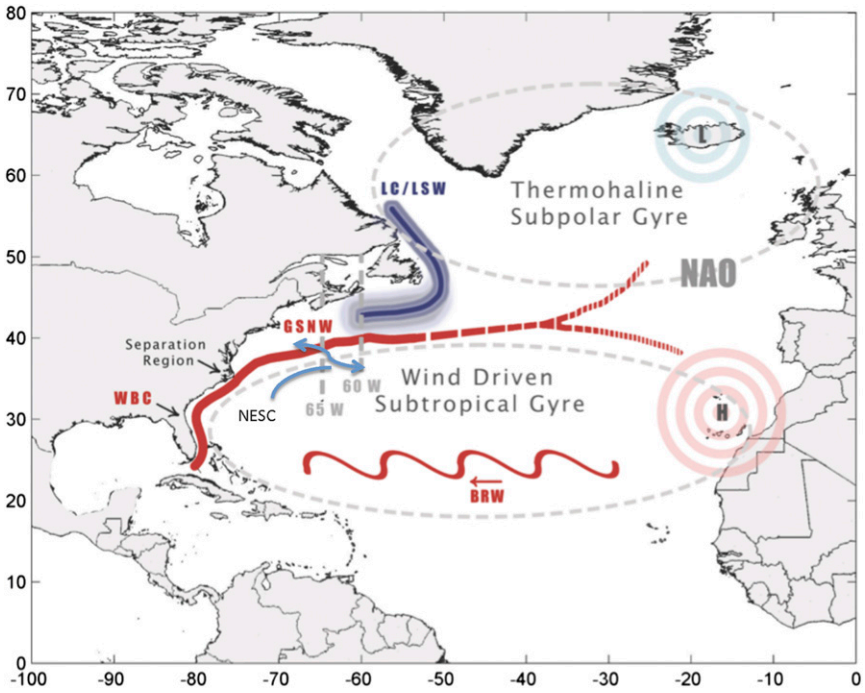

Figure 6. A synergistic perspective on the coupling between the Gulf Stream and the NAO. The GS (dark red line) is situated at the intergyre boundary between the subtropical and subpolar gyres. Its response is thus partly basin-scale wind-driven through long baroclinic Rossby waves (BRW) and partly influenced by buoyancy advection of LC and LSW from the Labrador Sea region. While the Azores high directly sets up the wind-driven gyre, the buoyancy impact from the subpolar gyre is centered on the Icelandic low, the two of which are components of the NAO. Note the spread of NESC (blue wiggly line) across the GS in the transition zone (65°–60°W), probably impacting/contributing to the changeover of temporal variability of the GS from west to the east.

First, let us consider the region between the separation point and 65°W. Here, the GS path behavior might be dominated by integrated basinwide wind effect, which forms the western boundary current and thus can be related to the NAO signal both at the near-decadal period and at the 2–3-yr band. In particular, Chaudhuri et al. (2011b) found that after the GS separates from the coast, diminished GS transport is seen (along with southern latitudinal excursion) during low NAO periods, which are accompanied by a weak DWBC, weak northern gyre, and weak southern gyre recirculation. The converse was true for the high NAO phases.

Additionally, the variability in this region might be a direct result of propagation of signal from the Labrador region (and related to NAO periods). Results from the Eden and Willebrand (2001) model suggest that enhanced heat loss due to severe winters witnessed in the Labrador Sea during high NAO periods result in stronger convection activity. These convection events are seen to induce baroclinic boundary wavelike structures traveling southward into the subtropical gyre and the GS system with time scales of 6–8 years. The enhanced

thermohaline circulation follows the crest of the baroclinic boundary wave. Thus, influence of the western GS system as seen from our study could be in response to NAO-induced, southward-traveling baroclinic boundary waves with time scales of 6–8 years.

Second, the region between 65° and 60°W can be considered a transition or mixed-response zone, where the wind-driven response to the west transitions to (and combines with) large-amplitude meandering variability to the east. Incidentally, this region overlies the New England Seamount Chain (NESC), which extends almost 800 km from Bear Seamount near Massachusetts (40°N, 67°W) to the Vogel Seamount (37°N, 60°W), with multiple high seamounts such as Kelvin and Manning Seamounts in between. The interaction of the GS meandering with this geologic feature that rises to about 1500 m at certain places is yet to be fully explored. Note also that the EOF analysis by Peña-Molino and Joyce (2008) did not show any contribution to the lowest EOF mode to the east of 60°W. To the east of 60°W, this near-decadal signal is absent and a new 4–5-yr signal is observed. While a similar 4–5-yr peak is observed in the NAO spectrum (Figure 4b), the reason for this in either time series is unclear at this time, and more investigation is warranted.

Third, there is the eastern segment between 60° and 50°W, where the stream meanders with a clear dominance of a 5-yr period. A recent observational study by Bower et al. (2009) presents a view that there are other interior pathways below 700 m for the North Atlantic Deep Water to reach the western boundary, contradicting the traditional concept of the DWBC carrying the LSW under the GS and affecting its path. This would further support the idea that the impact of LSW advection is probably limited to the surface layers and in the slope sea near the Grand Banks region north of the eastern section of the GS system. Thus, the response of the GS to the east of 60°W might be more influenced by the Labrador flow modified by the Icelandic low, ice melting from the Arctic, and other subarctic processes (interannual variability).

Furthermore, it is well known that the baroclinic recirculation to the south and the barotropic recirculation to the north add transport to the GS up to 60°W (Hogg 1992; Gangopadhyay et al. 1997; Chaudhuri et al. 2011a,b). This additional transport helps maximize the GS transport near 60°W (to about 150 Sv from about 90 Sv at Hatteras, near separation), east of which the transport diminishes as the subbasin-scale gyres extract mass from the GS to feed themselves in the recirculation process. Thus, one would expect that the behavior of the GS meandering to the west and to the east of 60°W might be somewhat different. Also, the GS interaction with the NESC (Cornillon et al. 1987) between 65° and 60°W results in large-amplitude meandering eastward. It is possible that the energy of meandering from the western side of the seamounts gets partitioned in a preferred way to result in the additional peak seen in the eastern (60°–50°W) spectra.

In summary, on the basis of the foregoing analyses, we hypothesize that 1) the near-decadal (~8 years) variability is a distinct feature of the GS system from 75° through 65°W and might be related to the NAO via integrated wind effects; and 2) to the east of 60°W, the GS responds with a different dominant interannual time scale of ~5 years, which might be (speculatively, at this time) related to the Labrador inflow, to other subpolar (ice melts) processes, and to large-amplitude meandering of the stream itself (due to its interactions with the New England seamounts) in the east. Interestingly, the nature of this temporal variability reflects

both continuity and evolution of the GS meandering path from Cape Hatteras to at least 50°W. Future work will entail testing these hypotheses by conducting process-based modeling experiments.

Acknowledgments. This work was partially supported by NASA's Interdisciplinary Science Grant NNG04GH50G, NSF Grants OCE-0815679 and OCE-0535379, and NOAA Grant NA11NOS0120038 [for the implementation of the Mid-Atlantic Regional Association Coastal Ocean Observing System (MARACOOS)]. Funding at AER was provided by NSF Grant ARC-1022733. We wish to thank Dr. Terry Joyce, WHOI, for kindly providing the GSNW index data (JQI). The model simulations were carried out at the NCAR Yellowstone Supercomputer Facility under NSF Project 0815679 (CISL P37921002). Dr. Andre Schmidt generated the GS path time series from AVISO data, while being supported under NOAA/MARACOOS award. We want to thank Mr. Frank Smith of SMAST for his editorial help during the final stages of the manuscript preparation. Finally, we wish to thank two anonymous reviewers for their thoughtful suggestions to a previous version of this manuscript, which substantially improved the analyses presented in this manuscript.

References

Bower, A. S., M. S. Lozier, S. F. Gary, and C. W. Boning, 2009: Interior pathways of the North Atlantic meridional overturning circulation. *Nature*, **459**, 243–247, doi:10.1038/nature07979.

Brown, O. B., P. Cornillon, S. R. Emerson, and H. M. Carle, 1986: Gulf Stream warm rings: A statistical study of their behavior. *Deep-Sea Res.*, **33**, 1459–1473, doi:10.1016/0198-0149(86)90062-2.

Burg, J. P., 1977: Maximum entropy spectral analysis. Ph.D. thesis, Stanford University, 123 pp.

Chaudhuri, A. H., A. Gangopadhyay, and J. J. Bisagni, 2011a: Contrasting response of the eastern and western North Atlantic circulation to an episodic climate event. *J. Phys. Oceanogr.*, **41**, 1630–1638, doi:10.1175/2011JPO4512.1.

——, ——, and ——, 2011b: Response of the western North Atlantic basin to characteristic high and low phases of the North Atlantic Oscillation. *Ocean Modell.*, **39**, 220–232, doi:10.1016/j.ocemod.2011.04.005.

Cook, E. R., R. D. D'Arrigo, and K. R. Briffa, 1998: The North Atlantic Oscillation and its expression in circum-Atlantic tree-ring chronologies from North America and Europe. *Holocene*, **8**, 9–17, doi:10.1191/095968398677793725.

Cornillon, P., 1986: The effect of the New England seamounts on Gulf Stream meandering as observed from satellite IR imagery. *J. Phys. Oceanogr.*, **16**, 386–389, doi:10.1175/1520-0485(1986)016<0386:TEOTNE>2.0.CO;2.

——, C. Gilman, L. Stramma, O. Brown, R. Evans, and J. Brown, 1987: Processing and analysis of large volumes of satellite-derived thermal infrared data. *J. Geophys. Res.*, **92**, 12 993–13 002, doi:10.1029/JC092iC12p12993.

Danabasoglu, G., J. C. McWilliams, and P. R. Gent, 1994: The role of mesoscale tracer transports in the global ocean circulation. *Science*, **264**, 1123–1126, doi:10.1126/science.264.5162.1123.

Dickson, R., J. Lazier, J. Meincke, P. Rhines, and J. Swift, 1996: Long-term coordinated changes in the convective activity of the North Atlantic. *Prog. Oceanogr.*, **38**, 241–295, doi:10.1016/S0079-6611(97)00002-5.

Drinkwater, K., 2004: Atmospheric and sea-ice conditions in the northwest Atlantic during the decade, 1991–2000. *J. Northwest Atl. Fish. Sci.*, **34**, 1–11, doi:10.2960/J.v34.m511.

——, B. Petrie, and P. C. Smith, 2003: Climate variability on the Scotian shelf during the 1990s. *ICES Mar. Sci. Symp.*, **219**, 40–49.

Eden, C., and J. Willebrand, 2001: Mechanism of interannual to decadal variability of the North Atlantic circulation. *J. Climate*, **14**, 2266–2280, doi:10.1175/1520-0442(2001)014<2266:MOITDV>2.0.CO;2.

Frankignoul, C., G. de Coetlogon, T. M. Joyce, and S. F. Dong, 2001: Gulf Stream variability and ocean–atmosphere interactions. *J. Phys. Oceanogr.*, **31**, 3516–3529, doi:10.1175/1520-0485(2002)031<3516:GSVAOA>2.0.CO;2.

Fratantoni, P. S., and R. S. Pickart, 2007: The western North Atlantic shelfbreak current system in summer. *J. Phys. Oceanogr.*, **37**, 2509–2533, doi:10.1175/JPO3123.1.

Gangopadhyay, A., P. Cornillon, and L. B. Jackson, 1989: Autoregressive modeling for spectral analysis of oceanographic data. *J. Geophys. Res.*, **94**, 16 215–16 226, doi:10.1029/JC094iC11p16215.

——, ——, and D. R. Watts, 1992: A test of the Parsons–Veronis hypothesis related to the separation of the Gulf Stream from the coast. *J. Phys. Oceanogr.*, **22**, 1286–1301, doi:10.1175/1520-0485(1992)022<1286:ATOTPH>2.0.CO;2.

——, A. R. Robinson, and H. G. Arango, 1997: Circulation and dynamics of the western North Atlantic. Part I: Multiscale feature models. *J. Atmos. Oceanic Technol.*, **14**, 1314–1332, doi:10.1175/1520-0426(1997)014<1314:CADOTW>2.0.CO;2.

Gent, P. R., and J. C. McWilliams, 1990: Isopycnal mixing in ocean circulation models. *J. Phys. Oceanogr.*, **20**, 150–155, doi:10.1175/1520-0485(1990)020<0150:IMIOCM>2.0.CO;2.

Griffies, S. M., A. Gnanadesikan, R. C. Pacanowski, V. Larichev, J. K. Dukowicz, and R. D. Smith, 1998: Isoneutral diffusion in a z-coordinate ocean model. *J. Phys. Oceanogr.*, **28**, 805–830, doi:10.1175/1520-0485(1998)028<0805:IDIAZC>2.0.CO;2.

Halkin, D., and T. Rossby, 1985: The structure and transport of the Gulf Stream at 73°W. *J. Phys. Oceanogr.*, **15**, 1439–1452, doi:10.1175/1520-0485(1985)015<1439:TSATOT>2.0.CO;2.

Hameed, S., and S. A. Piontkovski, 2004: The dominant influence of the Icelandic low on the position of the Gulf Stream northwall. *Geophys. Res. Lett.*, **31**, L09303, doi:10.1029/2004GL019561.

Hogg, N. G., 1992: On the transport of the Gulf Stream between Cape Hatteras and the Grand Banks. *Deep-Sea Res.*, **39**, 1231–1246, doi:10.1016/0198-0149(92)90066-3.

Hurrell, J. W., Y. Kushnir, G. Ottersen, and M. Visbeck, Eds., 2000: *The North Atlantic Oscillation: Climatic Significance and Environmental Impact*. *Geophys. Monogr.*, Vol. 134, Amer. Geophys. Union, 279 pp.

——, ——, and M. Visbeck, 2001: The North Atlantic Oscillation. *Science*, **291**, 604–605, doi:10.1126/science.1058761.

——, and Coauthors, Eds., 2014: The climate data guide: Hurrell North Atlantic Oscillation (NAO) index (station-based). NCAR/UCAR dataset, accessed 15 September 2014. [Available online at https://climatedataguide.ucar.edu/climate-data/hurrell-north-atlantic-oscillation-nao-index-station-based.]

Jackson, L. B., 1986: *Digital Filters and Signal Processing.* Kluwer Academic, 259 pp.

Jenkins, G. M., and D. G. Watts, 1968: *Spectral Analysis.* Prentice Hall, 523 pp.

Jones, P. D., T. Jonsson, and D. Wheeler, 1997: Extension to the North Atlantic Oscillation using early instrumental pressure observations from Gibraltar and south-west Iceland. *Int. J. Climatol.*, **17**, 1433–1450, doi:10.1002/(SICI)1097-0088(19971115)17:13<1433::AID-JOC203>3.0.CO;2-P.

Joyce, T. M., C. Deser, and M. A. Spall, 2000: On the relation between decadal variability of subtropical mode water and the North Atlantic Oscillation. *J. Climate*, **13**, 2550–2569, doi:10.1175/1520-0442(2000)013<2550:TRBDVO>2.0.CO;2.

——, Y.-O. Kwon, and L. Yu, 2009: On the relationship between synoptic wintertime atmospheric variability and path shifts in the Gulf Stream and Kuroshio Extension. *J. Climate*, **22**, 3177–3192, doi:10.1175/2008JCLI2690.1.

Kay, S. M., and S. L. Marple Jr., 1981: Spectrum analysis—A modern perspective. *Proc. IEEE*, **69**, 1380–1419, doi:10.1109/PROC.1981.12184.

Koslov, J. W., and R. H. Jones, 1985: A unified approach to confidence bounds for the autoregressive spectral estimator. *J. Time Ser. Anal.*, **6**, 141–151, doi:10.1111/j.1467-9892.1985.tb00405.x.

Lee, T., and P. Cornillon, 1996: Propagation and growth of Gulf Stream meanders between 75° and 45°W. *J. Phys. Oceanogr.*, **26**, 225–241, doi:10.1175/1520-0485(1996)026<0225:PAGOGS>2.0.CO;2.

Myers, R. A., J. Helbig, and D. Holland, 1989: Seasonal and interannual variability of the Labrador Current and West Greenland Current. ICES Rep. ICES CM 1989/C:16, 18 pp. [Available online at http://www.ices.dk/sites/pub/CM%20Doccuments/1989/C/1989_C16.pdf.]

Osborn, T., 2014: Tim Osborn: North Atlantic Oscillation index data. CRU datatset, accessed 15 September 2014. [Available online at http://www.cru.uea.ac.uk/~timo/datapages/naoi.htm.]

Parsons, A. T., 1969: A two-layer model of Gulf Stream separation. *J. Fluid Mech.*, **39**, 511–528, doi:10.1017/S0022112069002308.

Peña-Molino, B., and T. M. Joyce, 2008: Variability in the slope water and its relation to the Gulf Stream path. *Geophys. Res. Lett.*, **35**, L03606, doi:10.1029/2007GL032183.

Pickart, R. S., T. K. McKee, D. J. Torres, and S. A. Harrington, 1999: Mean structure and interannual variability of the slopewater system south of Newfoundland. *J. Phys. Oceanogr.*, **29**, 2541–2558, doi:10.1175/1520-0485(1999)029<2541:MSAIVO>2.0.CO;2.

Press, W. H., B. P. Flannery, S. A. Taukolsky, and W. T. Vetterling, Eds., 1986: *Numerical Recipes: The Art of Scientific Computing*. Cambridge University Press, 434 pp.

Rissanen, J., 1983: A universal prior for the integers and estimation by minimum description length. *Ann. Stat.*, **11**, 416–431, doi:10.1214/aos/1176346150.

Rossby, H. T., 1999: On gyre interactions. *Deep-Sea Res. II*, **46**, 139–164, doi:10.1016/S0967-0645(98)00095-2.

——, and R. L. Benway, 2000: Slow variations in the mean path of the Gulf Stream east of Cape Hatteras. *Geophys. Res. Lett.*, **27**, 117–120, doi:10.1029/1999GL002356.

Shchepetkin, A. F., and J. C. McWilliams, 2005: The Regional Oceanic Modeling System: A split-explicit, free-surface, topography-following-coordinate ocean model. *Ocean Modell.*, **9**, 347–404, doi:10.1016/j.ocemod.2004.08.002.

Smith, P. C., R. W. Houghton, R. G. Fairbanks, and D. G. Mountain, 2001: Interannual variability of boundary fluxes and water mass properties in the Gulf of Maine and on Georges Bank: 1993–1997. *Deep-Sea Res. II*, **48**, 37–70, doi:10.1016/S0967-0645(00)00081-3.

Song, Y., and D. B. Haidvogel, 1994: A semi-implicit ocean circulation model using a generalized topography-following coordinate system. *J. Comput. Phys.*, **115**, 228–244, doi:10.1006/jcph.1994.1189.

Spall, M. A., 1996: Dynamics of the Gulf Stream/deep western boundary current crossover. Part I: Entrainment and recirculation. *J. Phys. Oceanogr.*, **26**, 2152–2168, doi:10.1175/1520-0485(1996)026<2152:DOTGSW>2.0.CO;2.

Stommel, H., 1987: *A View of the Sea.* Princeton University Press, 165 pp.

Taylor, A. H., 2011: *The Dance of Air and Sea: How the Oceans, Weather and Life Link Together.* Oxford University Press, 288 pp.

——, and J. A. Stephens, 1998: The North Atlantic Oscillation and the latitude of the Gulf Stream. *Tellus*, **50**, 134–142, doi:10.1034/j.1600-0870.1998.00010.x.

——, and A. Gangopadhyay, 2001: A simple model of interannual shifts of the Gulf Stream. *J. Geophys. Res.*, **106**, 13 849–13 860, doi:10.1029/1999JC000147.

Thompson, J. D., and W. J. Schmitz Jr., 1989: A limited-area model of the Gulf Stream: Design, initial experiments, and model–data intercomparison. *J. Phys. Oceanogr.*, **19**, 791–814, doi:10.1175/1520-0485(1989)019<0791:ALAMOT>2.0.CO;2.

Tracey, K. L., and D. R. Watts, 1986: On the Gulf Stream meander characteristics near Cape Hatteras. *J. Geophys. Res.*, **91**, 7587–7602, doi:10.1029/JC091iC06p07587.

Veronis, G., 1973: Model of World Ocean circulation: 1. Wind-driven, two-layer. *J. Mar. Res.*, **31**, 228–288.

Walker, G. T., and E. W. Bliss, 1932: World weather V. *Mem. Roy. Meteor. Soc.*, **4**, 53–84.

Wunsch, C., 1999: The interpretation of short climate records, with comments on the North Atlantic and Southern Oscillations. *Bull. Amer. Meteor. Soc.*, **80**, 245–255, doi:10.1175/1520-0477(1999)080<0245:TIOSCR>2.0.CO;2.